Journal of Hazardous Materials 183 (2010) 116–124

Contents lists available at ScienceDirect

Journal of Hazardous Materials

journal homepage: www.elsevier.com/locate/jhazmat

Chemical characterization of dust particles recovered from bag filters of electric arc furnaces for steelmaking: Some factors influencing the formation of hexachlorobenzene

Naoto Tsubouchi*, Hiroyuki Hashimoto, Noriaki Ohtaka, Yasuo Ohtsuka

Research Center for Sustainable Materials Engineering, Institute of Multidisciplinary Research for Advanced Materials, Tohoku University, Katahira, Aoba-ku, Sendai 980-8577, Japan

ARTICLE INFO

Article history:
Received 16 February 2010
Received in revised form 29 June 2010
Accepted 30 June 2010
Available online 7 July 2010

Keywords:
Electric arc furnace steelmaking
Dust
Hexachlorobenzene
Active carbon sites
Surface zinc species

ABSTRACT

To make clear some factors controlling the formation of hexachlorobenzene (HCB) in the process of electric arc furnace (EAF) steelmaking, six dust samples recovered from different bag filters in commercial EAF steelmaking plants have been characterized with XRD, SEM-EPMA, XPS and temperature-programmed desorption (TPD) techniques. These dust samples contain 1.9–8.0 mass% of chlorine element, and the XPS and TPD measurements exhibit that the Cl is enriched at the dust surface and composed of the inorganic and organic functionalities, part of the Cl being evolved as HCl in the temperature region of flue gas treatment. All of the samples also include 2.1–6.4 mass% of carbon element, and some of the C can release CO_2 in the TPD up to 300 °C to form active carbon sites. The number is related closely to HCB concentration of each dust. Further, it is suggested that the Zn present in the samples consists of $ZnFe_2O_4$, ZnO and surface $ZnCO_3$, and the dust with a larger content of the $ZnCO_3$ has a higher concentration of HCB. It is possible that HCB formation occurs via gas–solid–solid interactions among gaseous Cl-containing compounds in flue gas, active carbon sites and surface Zn-species produced in exhaust ducts and bag filters.

1. Introduction

Some of the chlorine present in steel scrap and coke breeze is recognized to be involved in the formation of hazardous Cl-compounds, such as polychlorinated dibenzodioxins, polychlorinated dibenzofurans and hexachlorobenzene (denoted as HCB), in the process of electric arc furnace (EAF) steelmaking [1–6]. Although various studies using actual and model EAF dust samples have been carried out to elucidate possible mechanisms of the formation of the former two compounds [1–3,5], most of the researchers have paid no attention to HCB emitted in this process. It has recently been reported that HCB formation takes place around 300 °C, that is, at the cooling stage of flue gas after the EAF steelmaking [4,6].

According to previous work on the formation of organic chlorides including dioxins [7–10] and HCB [10], it is probable that these Cl-compounds released unintentionally from various industrial processes, such as waste incineration, iron ore sintering and EAF steelmaking, are produced mainly through *de novo* synthesis downstream after combustion. It has also been accepted that some metallic chlorides present in fly ashes and dust particles work as the catalysts for the synthesis around 300 °C [1–10]. It is of interest to examine the chemical forms and surface functionalities of Cl, C and metal species in EAF dust, because the results may contribute to the elucidation of the chemistry of HCB formation in exhaust ducts and bag filters. In this paper, therefore, we first examine the chemical states of the Cl, C and Zn present in dust particles formed in commercial EAF steelmaking processes with XRD, SEM-EPMA and XPS methods, then follow the changes upon heating treatment with a temperature-programmed desorption (TPD) technique, and finally make clear some factors controlling HCB formation in the process of flue gas treatment.

2. Experimental

2.1. Dust samples

Six kinds of dust samples recovered from bag filters in commercial, different EAF steelmaking facilities were supplied from the Japan Iron and Steel Federation and used in this work. Each sample was divided equally into about 1.0 g with a rotary splitter in a darkroom and stored in a N_2-filled plastic bag kept in a refrigerator. The average particle size or BET surface area of each dust was in the range of 5–10 μm or 20–50 m^2/g, respectively. Table 1 summarizes elemental compositions of the six samples investigated. As expected, Fe and Zn were the main elements, irrespective of the

* Corresponding author. Tel.: +81 22 217 5654; fax: +81 22 217 5655.
E-mail address: tsubon@tagen.tohoku.ac.jp (N. Tsubouchi).

0304-3894/$ – see front matter © 2010 Elsevier B.V. All rights reserved.
doi:10.1016/j.jhazmat.2010.06.122

Table 1
Elemental compositions of dust samples used.

Dust sample	Content (mass%-dry)															
	C[a]	N[a]	Na[b]	Mg[b]	Al[b]	Si[b]	S[a]	Cl[b]	K[b]	Ca[b]	Mn[b]	Fe[b]	Cu[b]	Zn[b]	Sn[b]	Pb[b]
A	2.5	0.03	1.7	0.69	2.1	1.4	0.31	6.6 (6.6)[c]	1.5	1.3	1.9	24.9	0.24	26.1	0.04	2.2
B	2.1	0.01	0.80	1.2	0.72	2.4	0.14	2.3 (2.3)[c]	0.51	3.0	2.8	41.4	0.14	10.8	0.02	0.72
C	6.4	0.12	1.4	2.0	1.8	2.3	0.68	6.5 (6.5)[c]	1.8	2.5	0.0	24.4	0.0	35.9	n.a.[d]	0.0
D	3.6	0.06	1.1	0.0	2.7	2.4	0.42	1.9 (1.9)[c]	1.4	2.8	1.3	34.9	0.0	26.7	n.a.[d]	0.0
E	3.1	0.04	3.0	0.0	1.0	2.1	0.55	8.0 (8.0)[c]	1.2	1.2	0.31	27.2	0.0	36.4	n.a.[d]	0.0
F	3.5	0.04	1.8	0.0	2.0	1.9	0.20	5.6 (5.6)[c]	1.5	1.3	0.0	30.3	0.0	25.1	n.a.[d]	0.0

[a] Determined with conventional, combustion-type elemental analyzers.
[b] Determined according to the Japanese Industrial Standard methods.
[c] Water-soluble chlorine.
[d] Not analyzed.

kind of the dust, and the corresponding contents ranged from 24 to 41 mass% and from 11 to 36 mass%. On the other hand, carbon and chlorine amounts were 2.1–6.4 and 1.9–8.0 mass%, respectively, and the latter values were always equal in the percent order to the contents (Table 1) of water-soluble Cl determined according to the Japanese Industrial Standard (JIS) Z 7302 method, but surface Cl-functionality is unclear. The concentrations of HCB in all dust samples were determined by the Soxhlet extraction/GC–MS method reported previously [6], and the reproducibility was within ±7% in every case.

2.2. XRD and SEM-EPMA analyses

The powder X-ray diffraction (XRD) measurements of as-received dust samples were conducted with an X-ray diffractometer (Shimadzu Corp.) using Ni-filtered Cu-Kα radiation (30 kV, 40 mA) to identify crystalline phases present in them. The average crystalline size of NaCl identified was determined by the Debye–Scherrer method.

Selected dust samples were also characterized with a scanning electron microscope (SEM) with an electron probe X-ray microanalyzer (EPMA) (JEOL, Ltd.) at a resolution of 6 nm and at an accelerating voltage of 15.0 kV.

2.3. XPS measurements

The X-ray photoelectron spectroscopy (XPS) analyses were performed with a non-monochromatic Mg-Kα X-ray source operating at 300 W (Kratos Analytical, Ltd.) to investigate the chemical forms of the chlorine and zinc on the surfaces of the dust samples. The analytical conditions have been reported in detail elsewhere [11,12] and are thus simply explained below. The sample was first pressed onto indium plate, then kept into the vacuum chamber for about 1 h to remove water and gas adsorbed, and finally introduced into the detector chamber under high vacuum ($2.0'10^{-7}$–$6.0'10^{-7}$ Pa) to start the XPS measurement. Long acquisition times of several hours were used to obtain good resolution for the Cl 2p and Zn 2p spectra, and their binding energies were referred to an In $3d_{5/2}$ peak of In_2O_3 at 444.9 eV.

Least-squares curve-fitting analyses of Cl 2p and Zn $2p_{3/2}$ spectra were made with a Gaussian/Lorentzian function. In the former case, the background-removed Cl spectrum was deconvoluted into inorganic and organic chlorides by assuming that the Cl $2p_{3/2}$ binding energies of both forms are equal to 198.5 eV [13,14] for NaCl and 200.5 eV [13,14] for C_6H_5Cl, respectively, and the energy difference (ΔE) between $2p_{3/2}$ and $2p_{1/2}$ is 1.60 eV, irrespective of the type of the chlorine [15]. The Zn $2p_{3/2}$ spectrum was deconvoluted into $ZnCO_3$ and other Zn-species, and the binding energies of $ZnCO_3$, ZnO and $ZnFe_2O_4$ were regarded to be 1022.5, 1021.8 and 1021.4 eV, respectively, on the basis of the reference data [13,14]. It has also been reported that several Zn compounds show the $2p_{1/2}$ peaks at 1043–1048 eV, and ΔE value between $2p_{3/2}$ and $2p_{1/2}$ is as large as about 23 eV, irrespective of the zinc type [13]. The detailed conditions of this curve-fitting method will be mentioned later (Fig. 6).

2.4. TPD runs

To investigate the thermal behavior of the carbon and chlorine in the dust and evaluate quantitatively active sites formed on the carbon surface, the samples used were subjected to the temperature-programmed desorption (TPD) experiments. All runs were conducted with a vertical, cylindrical flow-type quartz reactor. In the experiment, about 500 mg of each dust was first charged into the reactor, and special care was then taken to ensure that the whole reaction system was free from any leakage. After such prudent precautions, the sample was heated at 2 °C/min up to 300 °C in a stream of high-purity He (>99.99995%) or high-purity N_2 (>99.9995%). The details of the apparatus and procedure have been reported previously [16].

The concentration of CO_2 or CO desorbed in the TPD process was determined online at intervals of 2.5 min with a high-speed micro-gas chromatograph (GC) (Agilent Technologies, Inc.). Carbon active sites were calculated based on total amount of CO_2 evolved up to 300 °C. No appreciable amounts of CH_4 and C_2 hydrocarbons were detectable in any cases. With gaseous Cl-containing compounds, HCl was detected in situ at intervals of 1 min with a nondispersive infrared (IR) spectrometer (Thermo Environmental Instruments, Inc.), whereas Cl_2 was analyzed by the Gastec standard detector tube (Gastec Corp.) after collection of all the gas from the reactor exit [17–19].

3. Results and discussion

3.1. Chemical states of key elements at bulk and surface

Fig. 1 illustrates the XRD profiles of all dust samples examined. Magnetite (Fe_3O_4) or zinc ferrite ($ZnFe_2O_4$) was the dominant crystalline phase, irrespective of the type of the dust. The presence of these compounds has also been reported by the Mössbauer spectrum of an EAF dust with 49 mass% Fe and 9.2 mass% Zn [20]. As seen in Fig. 1, zincite (ZnO) existed in almost all of the samples. The XRD lines attributable to NaCl were detectable for the dust-A, C, E and F with relatively-large chlorine contents of 5.6–8.0 mass% (Table 1), and the average crystalline sizes were in the range of 40–60 nm. There may be some possibility about the NaCl sources. Inherent NaCl in steel scraps and coke breezes as raw materials, if present, may be considered as one possibility. According to thermodynamic calculations provided in Fig. 2a, the standard Gibbs free energy changes (ΔG) for the reactions (Eqs. (1)–(5)) of NaCl with H_2O, O_2 or CO_2 are as large as +25 to +63 kcal/mol at 1000–1500 °C

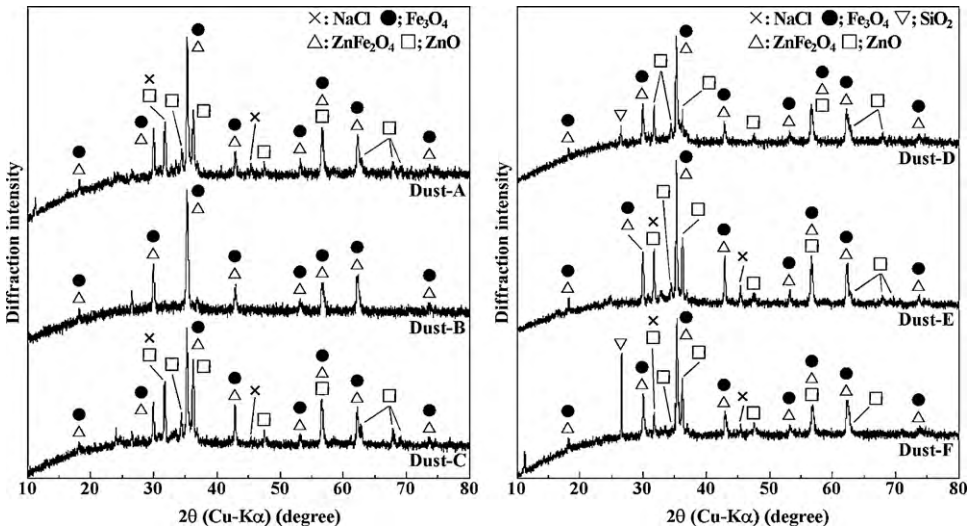

Fig. 1. XRD profiles for dust samples used.

close to typical EAF's temperature conditions.

$$NaCl + 0.5H_2O \rightarrow 0.5Na_2O + HCl \quad (1)$$

$$NaCl + H_2O \rightarrow NaOH + HCl \quad (2)$$

$$NaCl + 0.25O_2 \rightarrow 0.5Na_2O + 0.5Cl_2 \quad (3)$$

$$NaCl + 0.5CO_2 \rightarrow 0.5Na_2O + 0.5Cl_2 + 0.5CO \quad (4)$$

$$NaCl + CO_2 \rightarrow 0.5Na_2CO_3 + 0.5Cl_2 + 0.5CO \quad (5)$$

Thus, NaCl is very stable, showing that the NaCl identified in Fig. 1 may originate from the NaCl present in the raw materials. Another possibility may be secondary reactions of the Na-species in the dust and the raw materials with HCl (and/or Cl_2) once-evolved in the steelmaking process.

It is of interest to examine the chemical states of the chlorine at the surface of the samples used, which were thus supplied to the SEM-EPMA measurements. Fig. 3 illustrates the mapping profiles of Cl, Na, Zn and C elements in the dust-A or B. It seemed that Cl distribution was similar to the case of the Na or Zn element, irrespective of the dust type, and it could be overlaid partly with the map of the C element in each dust. Such a trend was also observed with the dust-C and D measured. These observations suggest that surface Cl-species in the four samples may be present as other forms than water-soluble inorganic chlorides, such as NaCl and $ZnCl_2$.

To make clear this point, the XPS analyses were carried out. Fig. 4 illustrates the Cl 2p XPS spectra of the six samples examined. Each spectrum observed, given by a solid line, was broad in the binding energy range of 196–203 eV, and it provided the main peak at 198–199 eV. It has been reported that the Cl $2p_{3/2}$ binding energies of inorganic chlorides (*e.g.* NaCl, $ZnCl_2$ and $FeCl_3$) and chlorobenzenes appear at about 198–199 and 200–201 eV, respectively [13,14]. Further, NaCl and 9-chloroanthracene ($C_{14}H_9Cl$) measured by the present XPS method gave the respective $2p_{3/2}$ peaks at 198.5 and 200.5 eV. It is thus evident that the chlorine on the outermost layers of these dust samples comprises both the inorganic and organic functionalities. To quantify separately these functional forms, all of the Cl 2p spectra measured were deconvoluted into inorganic and organic chlorides [11]. The results are shown as broken lines in Fig. 4, where the full width at half maximum (FWHM) value of each peak is assumed to be 1.6 eV on the basis of those observed for NaCl and $C_{14}H_9Cl$ as model compounds. Reasonable fit between the observed and curve-fitted spectra was obtained, and the reproducibility fell within ±3% in all cases. The deconvolution analysis exhibited that the proportion of organic C–Cl forms was in the range of 37–44 mol%.

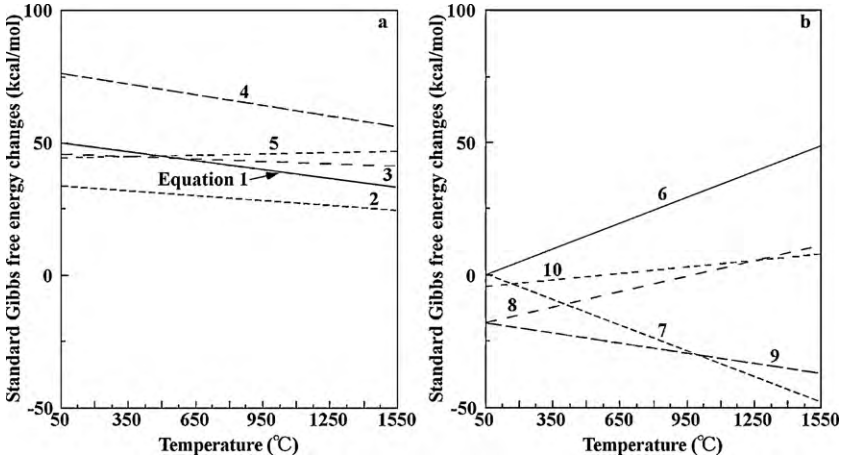

Fig. 2. Temperature dependence of standard Gibbs free energy changes for $NaCl + 0.5H_2O \rightarrow 0.5Na_2O + HCl$ (Eq. (1)), $NaCl + H_2O \rightarrow NaOH + HCl$ (Eq. (2)), $NaCl + 0.25O_2 \rightarrow 0.5Na_2O + 0.5Cl_2$ (Eq. (3)), $NaCl + 0.5CO_2 \rightarrow 0.5Na_2O + 0.5Cl_2 + 0.5CO$ (Eq. (4)), $NaCl + CO_2 \rightarrow 0.5Na_2CO_3 + 0.5Cl_2 + 0.5CO$ (Eq. (5)), $ZnO + CO_2 \rightarrow ZnCO_3$ (Eq. (6)), $ZnCO_3 \rightarrow ZnO + CO_2$ (Eq. (7)), $ZnO + 2HCl \rightarrow ZnCl_2 + H_2O$ (Eq. (8)), $ZnCO_3 + 2HCl \rightarrow ZnCl_2 + CO_2 + H_2O$ (Eq. (9)), $HCl + 0.25O_2 \rightarrow 0.5Cl_2 + 0.5H_2O$ (Eq. (10)).

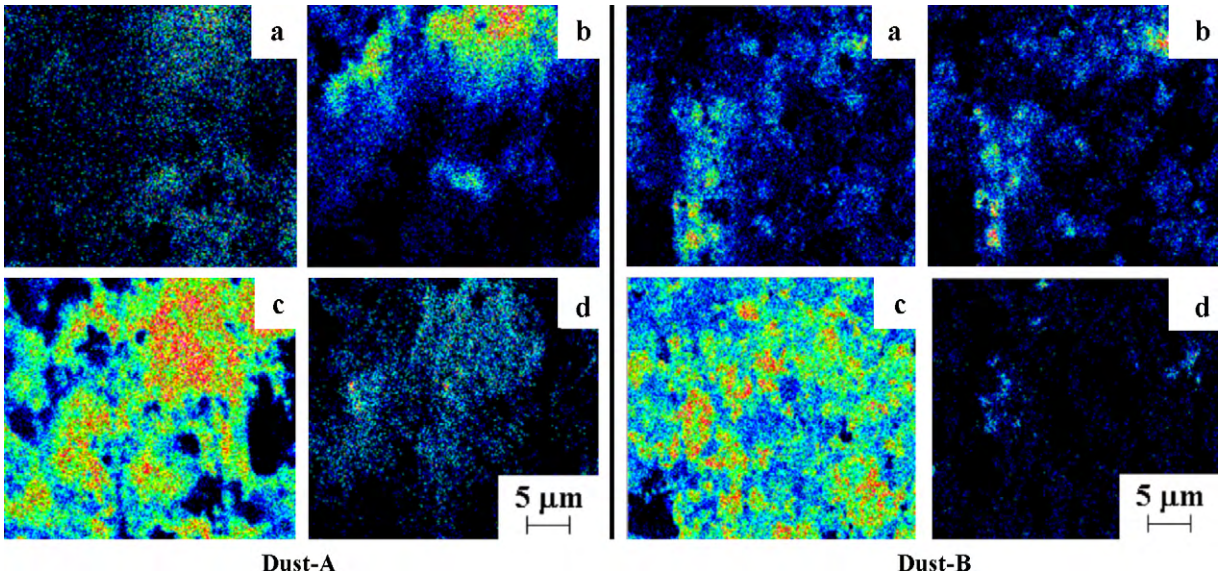

Fig. 3. SEM-EPMA pictures of dust-A and B: (a) chlorine, (b) sodium, (c) zinc and (d) carbon.

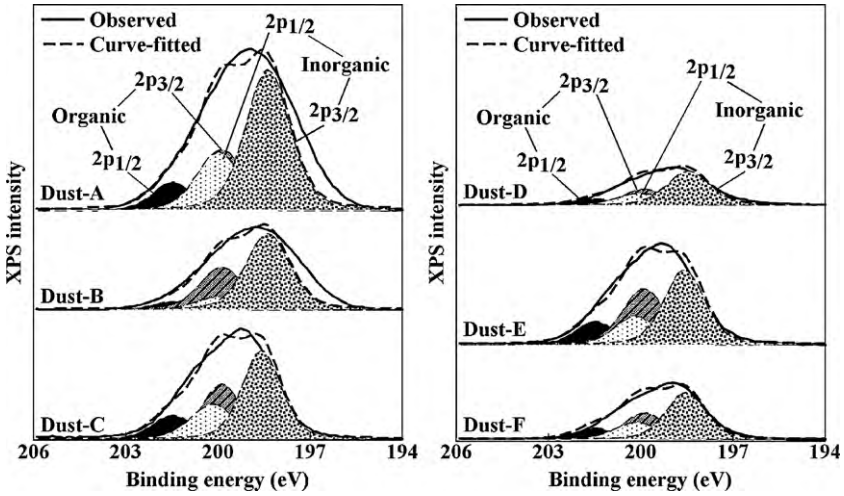

Fig. 4. Cl 2p XPS spectra for dust samples examined.

Table 2 presents atomic ratios of Cl/C, Zn/C and Fe/C in the dust samples. The Cl/C ratios determined by the XPS were 0.66–3.6, which were approximately 2–15 times those (0.18–0.91) obtained by elemental analysis and also larger than those (0.54–1.3) estimated by the SEM-EPMA. These results point out that the chlorine is enriched at the outermost layer of the dust surface. Since C–Cl forms could be observed only by the XPS analyses (Fig. 4), it is possible that active carbon sites and some metals present at the surface may play crucial roles in the formation of such Cl forms, which might be transformed partly into HCB in the process of flue gas treatment. With regard to Zn and Fe elements as the main components in the dust, as seen in Table 2, the Zn/C ratios were higher at a thinner surface layer, whereas the Fe/C ratios tended to be larger in the bulk.

Table 2
Atomic ratios of Cl/C, Zn/C and Fe/C in dust samples determined by XPS, SEM-EPMA methods and elemental analysis.

Dust sample	Atomic Cl/C ratio			Atomic Zn/C ratio			Atomic Fe/C ratio	
	XPS	SEM-EPMA	Elemental analysis	XPS	SEM-EPMA	Elemental analysis	XPS	Elemental analysis
A	1.8	1.3	0.91	2.8	2.2	2.0	0.38	2.2
B	1.6	1.0	0.36	3.2	2.9	0.91	0.48	4.2
C	0.66	0.54	0.34	2.6	1.8	1.0	0.17	0.83
D	2.5	0.74	0.18	2.4	1.7	1.4	2.6	2.1
E	2.7	n.a.[a]	0.86	2.7	n.a.[a]	2.1	0.67	1.9
F	3.6	n.a.[a]	0.54	3.0	n.a.[a]	1.3	1.5	1.9

[a] Not analyzed.

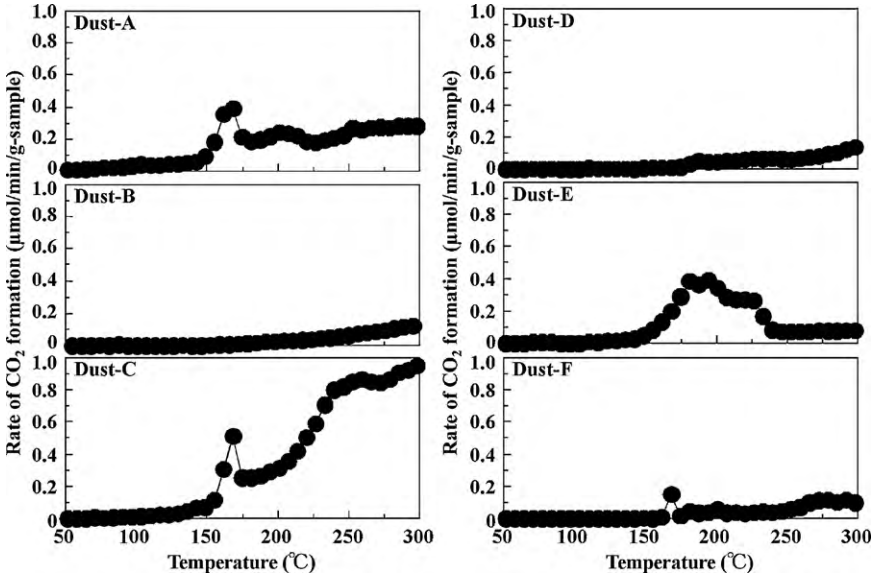

Fig. 5. Profiles for CO_2 formation from dust samples in the temperature-programmed desorption up to 300 °C.

3.2. Changes in chemical states of key elements upon heat treatment and determination of active carbon sites

The present authors' group has recently suggested that the number of active carbon sites derived from O-functional groups (for example, carboxyl/lactone/acid anhydride groups) on the surface of unburned carbon is one of the important factors controlling the extent of the formation of covalent C–Cl and C–F bonds [11,12].

To evaluate quantitatively the active sites formed from unburned carbon in the present dust in the temperature region of flue gas treatment, the samples used were heated up to 300 °C at a slow heating rate of 2 °C/min. The results are given in Fig. 5, where the rate of CO_2 formation is expressed as micromoles of CO_2 per minute and gram of feed dust. No measurable amounts of CO were detectable in all cases. CO_2 formation from the dust-A, C and E started apparently around 150 °C, and these samples showed the broad, distinct profiles with the sharp or shoulder peaks at about 165 °C. On the other hand, the CO_2 from the dust-B, D and F was very small. There may be some possibility about the sources of the CO_2 peak at 165 °C, and the decomposition of inorganic carbonates may be considered as one possibility. To examine this point, the TPD runs of commercially-available reagents, such as $CaCO_3$, $MnCO_3$, $CuCO_3{\cdot}Cu(OH)_2$ and $ZnCO_3$, were carried out in the same manner as in Fig. 5, and the results obtained showed that these compounds provided the CO_2 profiles peaking at 750, 430, 345 and 175 °C, respectively. It has also been reported that siderite ($FeCO_3$) can be converted to FeO and CO_2 between 400 and 600 °C [21]. Thus, the CO_2 peak around 165 °C in Fig. 5 was close to the decomposition temperature of the $ZnCO_3$. This observation indicates that $ZnCO_3$ in the dust-A, C and E, if present actually, may be transformed into ZnO and CO_2 at a lower temperature than bulk $ZnCO_3$, and the temperature difference may be due to the high dispersion of the $ZnCO_3$ in the three samples. On the other hand, the CO_2 observed beyond 200 °C (Fig. 5) with all dust samples originates probably from decomposition reactions of carboxyl (COOH) groups [22–24]. It is thus evident that each dust examined contains COOH groups, which can be transformed into active carbon sites and CO_2 in the temperature region of flue gas treatment.

The results of the TPD runs also suggest the presence of surface $ZnCO_3$ in the dust-A, C and E. To make sure this point, the Zn $2p_{3/2}$ XPS spectrum of each sample was measured. The results are illustrated in Fig. 6. As given in solid lines, the $2p_{3/2}$ spectra observed were broad in the binding energy range of 1018–1026 eV, irrespective of the kind of the dust, whereas the peak top values

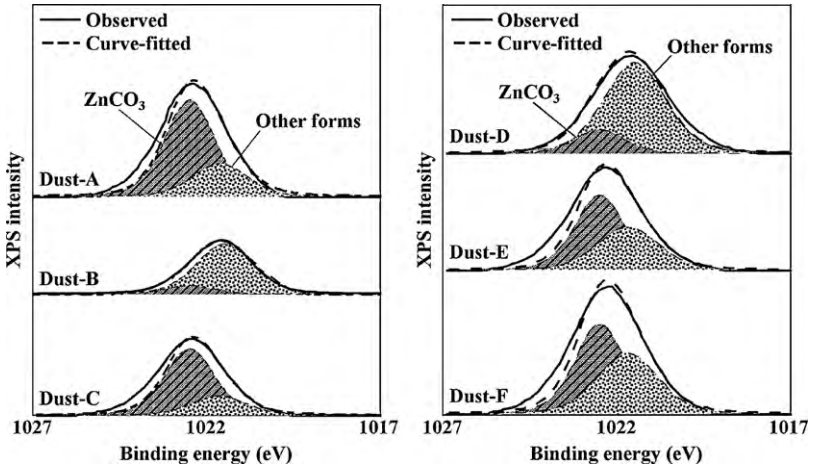

Fig. 6. Zn $2p_{3/2}$ XPS spectra for dust samples examined.

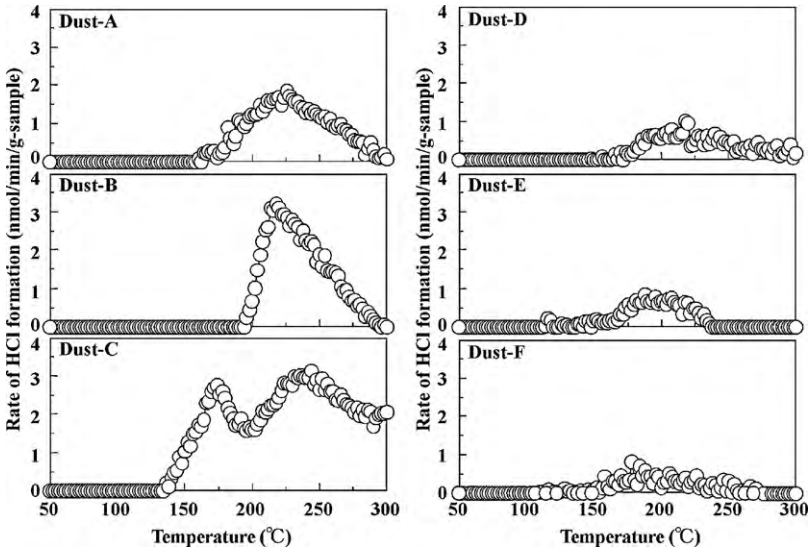

Fig. 7. Profiles for HCl formation from dust samples in the temperature-programmed desorption up to 300 °C.

were different among the samples. Since it has been reported that the Zn $2p_{3/2}$ binding energies of $ZnFe_2O_4$, ZnO and $ZnCO_3$ appear at 1021.4, 1021.8 and 1022.5 eV, respectively [25,26], the peak values with the dust-A, C, E and F were close to that of $ZnCO_3$. In addition, the XPS measurement of the dust-A after the TPD run showed the considerable decrease in the peak intensity around 1022 eV. Further, the four dust samples gave the CO_2 peaks at 165 °C during the TPD (Fig. 5), but no XRD lines of $ZnCO_3$ were detectable (Fig. 1). The combination of these results strongly suggests that the dust-A, C, E and F contain $ZnCO_3$, which is present only at the dust surface. To estimate the proportion of surface $ZnCO_3$ in the dust, all the Zn $2p_{3/2}$ spectra observed were curve-fitted with the least-squares method. The deconvolution results are given as broken lines in Fig. 6, where it is assumed that surface Zn-species other than $ZnCO_3$ have the $2p_{3/2}$ peak at 1021.6 eV, and the former FWHM value is varied between 1.9 and 2.1 eV to obtain the optimum curve resolution. The reproducibility of this curve-fitting analysis was ±1% in all cases, and the proportion of surface $ZnCO_3$ was calculated to be in the range of 13–75 mol%. When the proportion was plotted against organic C–Cl forms shown in Fig. 4, no distinct relationship was observed.

As shown in Figs. 1 and 6, the proportion of surface $ZnCO_3$ tended to be higher in the dust with a stronger diffraction intensity of ZnO(1 0 1) line at 2θ (Cu-Kα) of 36.3°. This observation might indicate that surface $ZnCO_3$ is formed via the reaction (Eq. (6)) of ZnO with CO_2 in flue gas at low temperatures of ≤165 °C (Fig. 5), and the extent of the occurrence of Eq. (6) depends strongly on the content of ZnO.

$$ZnO + CO_2 \rightarrow ZnCO_3 \quad (6)$$

The rate profiles of HCl formation in the TPD runs at 2 °C/min are shown in Fig. 7, where the rate is expressed as nanomoles of HCl per minute and gram of feed sample. The average concentration of HCl evolved was in the range of 0.55–1.2 ppm, and the shape of each profile observed was reproducible when the run was repeated at least twice. As given in Fig. 7, the HCl formation started at 140–160 °C in many cases, and the five samples except the dust-C exhibited the broad profiles with the peak temperature between 180 and 230 °C. On the other hand, the dust-C provided two distinct peaks at 175 and 235 °C. Appreciable amounts of Cl_2 could not be detected by the Gastec standard detector tube with all samples. As described above, surface $ZnCO_3$ is likely to be present in the dust-A, C, E and F. Since the $ZnCO_3$ can be decomposed into ZnO and CO_2 at about 165 °C (Fig. 5) according to Eq. (7), ZnO may react with HCl in flue gas and/or from the dust to provide $ZnCl_2$ (Eq. (8)).

$$ZnCO_3 \rightarrow ZnO + CO_2 \quad (7)$$

$$ZnO + 2HCl \rightarrow ZnCl_2 + H_2O \quad (8)$$

As seen in Fig. 2b, ΔG values for Eq. (8) at 100–300 °C are −19 to −13 kcal/mol, which means that this reaction is favorable thermodynamically under the temperature conditions of exhaust ducts and bag filters. $ZnCl_2$ may also be formed through the direct reaction of HCl in flue gas with the $ZnCO_3$ at low temperatures of ≤150 °C before its decomposition (Eq. (9)).

$$ZnCO_3 + 2HCl \rightarrow ZnCl_2 + CO_2 + H_2O \quad (9)$$

The ΔG values for Eq. (9) at 100–150 °C are −18 to −19 kcal/mol (Fig. 2b), indicating significant driving forces for $ZnCl_2$ formation. Although one may think that the dust-derived HCl is one of the Cl-sources for this reaction, the possibility is probably minor, because the amount of HCl evolved below 150 °C is negligibly small, regardless of the kind of the dust (Fig. 7). In addition, no appreciable amounts of CO_2 were detectable in this temperature region in many cases (Fig. 5).

To examine the possibility of $ZnCl_2$ formation via Eq. (9), the dust-A was exposed to a flow of 100 ppm HCl/N_2 at 120 °C where no release of HCl and CO_2 from this dust took place as seen in Figs. 5 and 7. The results revealed not only the decrease in HCl concentration but also the predominant evolution of CO_2 at the initial stage of the exposure process. Total amount of the HCl decreased or CO_2 evolved was estimated to be 520 or 1.2 μmol/g, respectively, and the latter value was close to the amount (1.6 μmol/g) of the CO_2 peak observed at 165 °C with the dust-A (Fig. 5). These observations suggest that Eq. (9) is possible in flue gas systems of actual EAF plants, though the HCl decreased was larger due probably to the physisorption at the dust surface, compared with the CO_2 evolved.

Cumulative amount of CO_2 or HCl evolved during the TPD can be estimated by integrating a corresponding rate profile shown in Figs. 5 or 7, respectively. The results are summarized in Table 3, where the average value of the two repeated experiments is provided. Total amounts of CO_2 from the six dust samples were in the range of 3.6–41 μmol/g, and the highest value observed with the dust-C was approximately 12 times the lowest one with the dust-B. On the other hand, the amount of the CO_2 peak at about 165 °C (Fig. 5) assigned to the decomposition of surface $ZnCO_3$ was 1.6,

Table 3
Cumulative amounts of CO_2 and HCl evolved in the temperature-programmed desorption of dust samples and the HCB concentrations.

Dust sample	CO_2 (μmol/g)[a]	HCl (nmol/g)[a]	HCB concentration (ng/g)[b]
A	18 (1.2 C-%)[c]	61 (5.2×10^{-3} Cl-%)[d]	64 (1.3)[e]
B	3.6 (0.26 C-%)[c]	81 (14×10^{-3} Cl-%)[d]	0.0
C	41 (1.0 C-%)[c]	170 (10×10^{-3} Cl-%)[d]	21 (0.43)[e]
D	4.5 (0.19 C-%)[c]	28 (4.9×10^{-3} Cl-%)[d]	0.0
E	10 (0.59 C-%)[c]	21 (1.1×10^{-3} Cl-%)[d]	20 (0.43)[e]
F	3.8 (0.22 C-%)[c]	17 (1.3×10^{-3} Cl-%)[d]	3.8 (0.078)[e]

[a] Average value of the repeated experiments.
[b] Determined according to the Soxhlet extraction/GC–MS method [6].
[c] Percent of total carbon in feed sample.
[d] Percent of total chlorine in feed sample.
[e] Expressed in C-nmol/g.

1.4, 1.5 or 0.43 μmol/g for the dust-A, C, E or F, respectively, and the proportion of the $ZnCO_3$ as the CO_2 source was calculated to be only 3–15%. These results point out that the number of active carbon sites produced in the temperature region of flue gas treatment depends strongly on the kind of the dust. As shown in Table 3, total amounts of HCl desorbed were in the range of 17–170 nmol/g, which corresponded to be 0.001–0.014 Cl-% of total chlorine and were much smaller than those (3.6–41 μmol/g) of CO_2.

Table 3 also shows the concentrations of HCB in the dust samples. HCB could be detected for the dust-A, C, E and F, and the concentration range was 3.8–64 ng/g (0.013–0.22 nmol/g). Since these dust samples release relatively-large amounts of CO_2 in the TPD experiments (Fig. 5 and Table 3) and contain surface $ZnCO_3$ (Figs. 5 and 6), active carbon sites produced after the CO_2 evolution and/or ZnO derived from the $ZnCO_3$ may affect HCB formation. The next section thus focuses on discussing this point in detail.

3.3. Several factors determining the formation of hexachlorobenzene

The concentration of HCB is plotted as a function of the number of active carbon sites in Fig. 8, where the latter is calculated by subtracting CO_2 derived from surface $ZnCO_3$ from total CO_2 amount (Table 3). There was an almost linear correlation between the two except the dust-C. Since the carbon sites arise predominantly from carboxyl groups as mentioned in Fig. 5, it is likely that –COOH-derived sites can play an important role in HCB formation. The reason for the largest deviation observed for the dust-C is unclear, but the sites observed with this sample might include the contribution of surface O-forms other than COOH groups, for examples, lactones, which might be converted partly to active sites and CO_2 below 300 °C with the dust-C (Fig. 5) by the catalysis of some minerals and trace elements present in the sample.

As shown in Table 3, the HCB concentration was the largest (64 ng/g) with the dust-A, and the value corresponded to be 1.3 C-nmol/g, which was four orders of magnitude lower than the number (18 C-μmol/g) of the active sites, suggesting that only part of them may be transformed into HCB. Such a trend was also observed with the dust-C, E and F. These observations may indicate the importance of Cl-sources in the HCB formation.

To discuss this point further, the concentration is then plotted as a function of the total amount (Table 3) of HCl desorbed in Fig. 9. Compared with the results in Fig. 8, no distinct correlation could be deduced. This might be ascribed to the contribution of Cl_2 other than the HCl desorbed to HCB formation, because part of HCl might be converted to Cl_2 with much higher chlorination activity via the Deacon reaction (Eq. (10) in Fig. 2b), which is more favorable thermodynamically at a lower temperature (Fig. 2b) and can be catalyzed by some minerals present in fly ashes under the temperature conditions of flue gas treatment [27,28].

Fig. 10 presents the HCB concentration as a function of the content of surface $ZnCO_3$ shown by TPD. The concentration was higher at a larger content of the $ZnCO_3$. On the other hand, there was no distinct relationship between the HCB and the Zn content determined

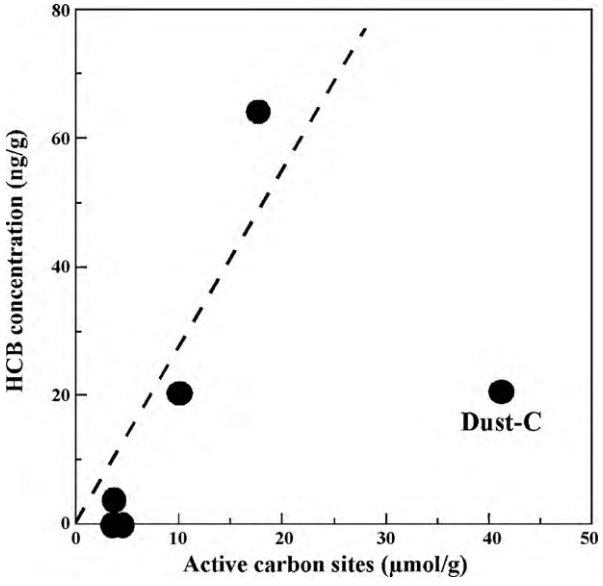

Fig. 8. Relationship between active carbon sites and HCB concentrations in dust samples.

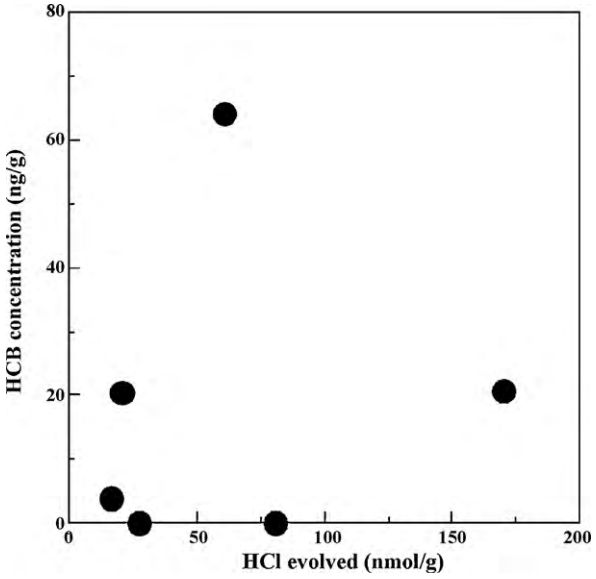

Fig. 9. HCB concentration in dust samples against total amount of HCl released up to 300 °C.

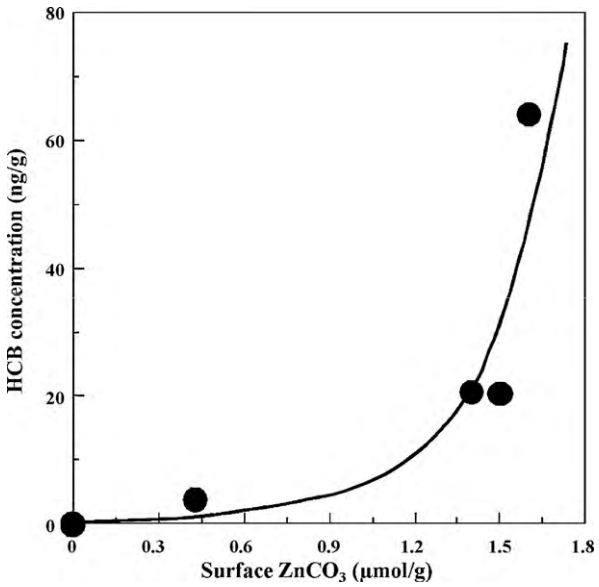

Fig. 10. Relationship between surface $ZnCO_3$ contents and HCB concentrations in dust samples.

by the chemical analysis in Table 1. The present authors' group has recently shown that HCl can interact physically and chemically with active carbon sites in activated carbon at 100–300 °C, and the extent of the interaction increases by doping Zn^{2+} ions to the carbon. In addition, the XPS measurements of the Zn-doped carbon exhibited the formation of covalent C–Cl bonds and $ZnCl_2$. It is thus possible that part of surface $ZnCO_3$ in the dust samples reacts with HCl in flue gas and/or from the dust through Eq. (9) (or Eqs. (7) and (8) at ≥150 °C) to be transformed into surface $ZnCl_2$, which may promote HCB formation. It has been reported that $ZnCl_2$ added on dust particles and model fly ashes can work as the catalyst for *de novo* synthesis of chlorinated organic compounds including HCB [6,29].

On the basis of the above-mentioned discussion, it may be reasonable to see that HCB formation occurs via interactions among HCl (and/or Cl_2) in flue gas, active carbon sites and surface $ZnCl_2$ formed in exhaust ducts and bag filters. In this process, the HCl may react with the active sites derived from COOH groups in the dust samples to produce Cl-containing intermediates, for example, HCl chemisorbed and/or surface HCl species, which might subsequently be converted to organic chlorides including HCB. The role of surface $ZnCO_3$ provided by TPD (Fig. 5) and XPS (Fig. 6) in HCB formation is not clear at present, but surface $ZnCl_2$ derived from Eqs. (7) and (8) (and/or Eq. (9)), if it can be actually produced, might catalyze the transformation of HCl into the Cl-containing intermediates and subsequently into HCB.

4. Conclusions

Six dust samples recovered from bag filters of electric arc furnaces for steelmaking are characterized by means of XRD, SEM-EPMA, XPS and TPD techniques to examine several factors controlling HCB formation in the steelmaking process. The dust samples include 1.9–8.0 and 2.1–6.4 mass% of Cl and C elements, respectively, and the Cl is enriched at the outermost layer of the dust surface and composed of the inorganic and organic functionalities. On the other hand, part of the C can release CO_2 in the TPD up to 300 °C to provide active carbon sites. Further, it is suggested that some of the dust samples contain surface $ZnCO_3$, which can readily be transformed into ZnO and CO_2 at about 165 °C. As the amount of the carbon sites or the $ZnCO_3$ increases, the concentration of HCB in the dust tends to increase. It may thus be reasonable to suppose that these amounts are important as the factors for determining the HCB formation.

Acknowledgments

This work was supported by the Steel Industry Foundation for the Advancement of Environmental Protection Technology (SEPT). The authors are grateful to Prof. Eiki Kasai of our Institute for his helpful discussion and suggestions. The assistance of Mr. Akiyuki Kawashima and Mr. Yuuki Akama in carrying out experiments is also acknowledged.

References

[1] W.S. Lee, G.P. Chang-Chien, L.C. Wang, W.J. Lee, K.Y. Wu, P.J. Tsai, Emissions of polychlorinated dibenzo-*p*-dioxins and dibenzofurans from stack gases of electric arc furnaces and secondary aluminum smelters, J. Air Waste Manage. Assoc. 55 (2005) 219–226.
[2] S.L. Figueira, J.F.P. Gomes, Emissions of dioxin and dibenzofuran from electric arc furnaces, Rev. Metal. 41 (2005) 164–168.
[3] M.B. Chang, H.C. Huang, S.S. Tsai, K.H. Chi, G.P. Chang-Chien, Evaluation of the emission characteristics of PCDD/Fs from electric arc furnaces, Chemosphere 62 (2006) 1761–1773.
[4] T. Öberg, Low-temperature formation and degradation of chlorinated benzenes, PCDD and PCDF in dust from steel production, Sci. Total Environ. 382 (2007) 153–158.
[5] J.F.P. Gomes, Emissions of polycyclic aromatic hydrocarbons and polycyclic carbonyl biphenyls from electric arc furnaces, Rev. Metal. 44 (2008) 280–284.
[6] T. Murakami, M. Shimura, E. Kasai, Formation of hexachlorobenzene from dusts of an electric arc furnace used in steelmaking: Effect of temperature and dust composition, Environ. Sci. Technol. 42 (2008) 7459–7463.
[7] G. McKay, Dioxin characterization, formation and minimization during municipal solid waste (MSW) incineration: review, Chem. Eng. J. 86 (2002) 343–368.
[8] S. Kuzuhara, E. Kasai, Formation of PCDD/Fs during oxidation of carbonaceous materials at low temperatures, Tetsu To Hagane, J. Iron Steel Inst. Jpn. 89 (2003) 811–818.
[9] M. Altarawneh, B.Z. Dlugogorski, E.M. Kennedy, J.C. Mackie, Mechanisms for formation, chlorination, dechlorination and destruction of polychlorinated dibenzo-*p*-dioxins and dibenzofurans (PCDD/Fs), Prog. Energy Combust. Sci. 35 (2009) 245–274.
[10] T. Öberg, T. Öhrström, J. Bergström, Metal catalyzed formation of chlorinated aromatic compounds: A study of the correlation pattern in incinerator fly ash, Chemosphere 67 (2007) S185–S190.
[11] N. Tsubouchi, E. Kasai, K. Kawamoto, H. Noda, Y. Nakazato, Y. Ohtsuka, Functional forms of carbon and chlorine in dust samples formed in the sintering process of iron ores, Tetsu To Hagane, J. Iron Steel Inst. Jpn. 91 (2005) 751–756.
[12] N. Tsubouchi, H. Hayashi, A. Kawashima, M. Sato, N. Suzuki, Y. Ohtsuka, Functional forms of the fluorine and carbon in fly ashes recovered from electrostatic precipitators of pulverized coal-fired plants, Fuel, submitted for publication.
[13] J.F. Moulder, W.F. Stichle, P.E. Sobol, K.D. Bomben, in: J. Chastain (Ed.), Handbook of X-ray Photoelectron Spectroscopy, Perkin-Elmer, Eden Praine, 1992.
[14] C.D. Wagner, A.V. Naumkin, A. Kraut-Vass, J.W. Allison, C.J. Powell, J.R. Rumble Jr., In NIST X-ray Photoelectron Spectroscopy Database Version 3.5 (Web version), NIST, Gaithersburg, 2007.
[15] J.E. Schaff, J.T. Roberts, Adsorbed states of acetonitrile and chloroform on amorphous and crystalline ice studied with X-ray photoelectron spectroscopy, Surf. Sci. 426 (1999) 384–394.
[16] N. Tsubouchi, S. Kuzuhara, E. Kasai, H. Hashimoto, Y. Ohtsuka, Properties of dust particles sampled from windboxes of an iron ore sintering plant: surface structures of unburned carbon, ISIJ Int. 46 (2006) 1020–1026.
[17] N. Tsubouchi, S. Ohtsuka, H. Hashimoto, Y. Ohtsuka, Several distinct types of HCl evolution during temperature-programmed pyrolysis of high-rank coals with almost the same carbon contents, Energy Fuels 18 (2004) 1605–1606.
[18] N. Tsubouchi, S. Ohtsuka, Y. Nakazato, Y. Ohtsuka, Formation of hydrogen chloride during temperature-programmed pyrolysis of coals with different ranks, Energy Fuels 19 (2005) 554–560.
[19] M. Takeda, A. Ueda, H. Hashimoto, T. Yamada, N. Suzuki, M. Sato, N. Tsubouchi, Y. Nakazato, Y. Ohtsuka, Fate of the chlorine and fluorine in a sub-bituminous coal during pyrolysis and gasification, Fuel 85 (2006) 235–242.
[20] J.G.M.S. Machado, F.A. Brehm, C.A.M. Moraes, C.A. dos Santos, A.C.F. Vilela, J.B.M. da Cunha, Chemical, physical, structural and morphological characterization of the electric arc furnace dust, J. Hazard. Mater. 136 (2006) 953–960.
[21] P.K. Gallagher, S.St.J. Warne, Thermomagnetometry and thermal decomposition of siderite, Thermochim. Acta 43 (1981) 253–267.
[22] Y. Otake, R.G. Jenkins, Characterization of oxygen-containing surface complexes created on a microporous carbon by air and nitric acid treatment, Carbon 31 (1993) 109–121.
[23] Q.-L. Zhuang, T. Kyotani, A. Tomita, The change of TPD pattern of O_2-gasified carbon upon air exposure, Carbon 32 (1994) 539–540.
[24] U. Zielke, K.J. Huttinger, W.P. Hoffman, Surface-oxidized carbon fibers: I. Surface structure and chemistry, Carbon 34 (1996) 983–998.

[25] C. Battistoni, J.L. Dormann, D. Fiorani, E. Paparazzo, S. Viticoli, X.P.S. An, Mössbauer study of the electronic properties of $ZnCr_XGa_{2-X}O_4$ spinel solid solutions, Solid State Commun. 39 (1981) 581–585.
[26] L.S. Dake, D.R. Baer, J.M. Zachara, Auger parameter measurements of zinc compounds relevant to zinc transport in the environment, Surf. Interface Anal. 14 (1989) 71–75.
[27] H. Hagenmaler, M. Kraft, H. Brunner, R. Haag, Catalytic effects of fly ash from waste incineration facilities on the formation and decomposition of polychlorinated dibenzo-*p*-dioxins and polychlorinated dibenzofurans, Environ. Sci. Technol. 21 (1987) 1080–1084.
[28] E.W.B. de Leer, R.J. Lexmond, M.A. de Zeeuw, "De novo"-synthesis of chlorinated biphenyls, dibenzofurans and dibenzo-*p*-dioxins in the fly ash catalyzed reaction of toluene with hydrochloric acid, Chemosphere 19 (1989) 1141–1152.
[29] L Stieglitz, H. Vogg, G. Zwick, J. Beck, H. Bautz, On formation conditions of organohalogen compounds from particulate carbon of fly ash, Chemosphere 23 (1991) 1255–1264.